PAPER

Time-synchronized continuous wave laser-induced fluorescence axial velocity measurements in a diverging cusped field thruster

IOP Publishing Journal of Physics D: Applied Physics
J. Phys. D: Appl. Phys. **47** (2014) 115204 (9pp) doi:10.1088/0022-3727/47/11/115204

Time-synchronized continuous wave laser-induced fluorescence axial velocity measurements in a diverging cusped field thruster

N A MacDonald[1,2], M A Cappelli[1] and W A Hargus Jr[2]

[1] Stanford Plasma Physics Laboratory, Stanford University, Stanford, CA 94305, USA
[2] In-Space Propulsion Branch, Air Force Research Laboratory, Edwards AFB, CA 93524, USA

E-mail: natalia.macdonald@us.af.mil

Received 8 November 2013, revised 10 January 2014
Accepted for publication 27 January 2014
Published 26 February 2014

Abstract

Measurements are presented of time-synchronized axial ion velocities at three positions in the discharge channel and plume of a diverging cusped field thruster operating on xenon. Xenon axial ion velocities for the thruster are derived from laser-induced fluorescence measurements of the $5d[4]_{7/2}$–$6p[3]_{5/2}$ xenon ion excited state transition centred at $\lambda = 834.72$ nm. The thruster is operated in a high-current mode, where the anode discharge current is shown to oscillate quasi-periodically. A sample-hold scheme is implemented to correlate ion velocities to phases along the current cycle. These time-synchronized measurements show that median axial ion velocities decrease as discharge current increases, and that the widths of ion velocity distributions increase with increases in discharge current for positions at the exit plane and outside the thruster channel.

Keywords: laser-induced fluorescence, time-resolved, plasmas, propulsion, laser diagnostics

(Some figures may appear in colour only in the online journal)

1. Introduction

Recent efforts in the satellite community to reduce spacecraft size and cost have sparked interest in scaling current plasma propulsion technologies to low power. Hall thrusters are one of the few plasma propulsion devices that have shown promise for accommodating a low power regime. However, issues such as increased sputtering and heat flux to channel walls arise when Hall thrusters are scaled down [1, 2], resulting in reduced lifetime. To lessen these scaling issues, several new cusped field plasma thrusters are being developed [3–6]. By removing the centre magnetic pole piece characteristic of annular Hall thrusters, and altering the magnetic field configuration, these cusped field thrusters reduce plasma impingement on channel walls and thereby minimize insulator erosion. This work focuses on one variant of the cusped field thruster, the Massachusetts Institute of Technology (MIT) developed diverging cusped field thruster (DCFT) [5]. This thruster has shown great promise in the <200 W power regime, with anode efficiencies on the order of 40% [5].

One useful measure of performance for these propulsion devices is ion velocity. The ion exhaust velocity is directly proportional to the thrust produced by these devices. Changes in velocity throughout the discharge can provide important information about propellant acceleration mechanisms and can indicate loss mechanisms. High spatial resolution of ion velocity measurements is critical in validating numerical simulations of these discharges, and can aid in future development efforts. A powerful diagnostic for ion velocimetry is laser-induced fluorescence (LIF). LIF provides the opportunity to probe small plasma sources with higher spatial resolution (typically <1 mm^2) than can be obtained with intrusive probes such as retarding potential analysers.

This work is motivated by previous time-averaged LIF velocimetry measurements on the DCFT [7]. The DCFT tends to operate in two modes: a high-current mode, characterized

by quasi-periodic discharge current oscillations; and a low-current mode that is quiescent [8]. Differences in the time-averaged velocity maps between the two modes include the presence of a widely distributed acceleration region and diffuse plume during the high-current mode that are not present in the low-current mode. While time-averaged measurements provide a good representation of the ion velocities throughout a quiescent discharge, they do not explain the additional physics underlying the high-current mode's discharge oscillations. A time-dependent velocity diagnostic is therefore necessary for resolving the ion dynamics.

This paper provides results of time-synchronized LIF velocimetry of an oscillatory cusped field plasma discharge operating on xenon. A continuous wave (CW) diode laser is used to probe the $5d[4]_{7/2}$–$6p[3]_{5/2}$ xenon ion excited state transition centred at $\lambda = 834.72$ nm. A sample-hold circuit and lock-in amplifier are used to extract fluorescence excitation lineshapes that each correspond to a particular point in time along the quasi-periodic discharge current cycle.

Time-resolved LIF measurements typically employ pulsed dye lasers to study properties such as the spectral line broadening of a given transition, reflecting the temperature, velocity distribution, etc [9]. However, the discharge in this work is operated on xenon, which has spectral linewidths that are too narrow to be resolved with a pulsed dye laser. The $5d[4]_{7/2}$–$6p[3]_{5/2}$ xenon ion transition used in this work has a measured linewidth (a convolution of the natural linewidth of the transition and the velocity distribution function (VDF) for a given time in the discharge current cycle) on the order of 1.5–2.5 GHz. Stat-of -the-art pulsed dye lasers have linewidths >1 GHz [10] at best. In comparison, CW lasers with linewidths <300 kHz [10] are sufficiently narrow to resolve the transition's spectral features, and are therefore more desirable for making time-synchronized fluorescence measurements.

In recent years, several studies have attempted time-resolved CW-LIF measurements in oscillatory plasma discharges such as Hall thrusters. These include measurements of the time evolutions of ion velocity profiles for a Hall thruster after short interruptions to the thruster discharge power [11, 12], or whose oscillations are driven at a particular frequency by a variable cathode current injection [13]. Our method [14, 15] varies from these studies in several important ways. First, it is intended for use on a quasi-periodic oscillatory mode of the DCFT discharge, operated continuously and without any alteration to the naturally occurring frequency. The oscillations in the DCFT are a result of the accumulation of ions within the thruster channel and subsequent expulsion of the ions due to an applied electric field. Without being driven at a constant frequency, these oscillations are quasi-periodic, with a frequency that tends to drift slightly over the course of a laser scan. Second, by using phase sensitive detection that is locked to a fixed mechanical chopper frequency, and a sample-hold circuit that triggers time synchronization when the discharge current passes through a particular level, not at a particular frequency, we are able to extract fluorescence signals correlated to discharge currents that are not perfectly periodic. In contrast, the photon-counting technique used in the aforementioned studies [16] is more reliant on the periodicity of the discharge oscillations due to the straight addition and subtraction of fluorescence and background photons, respectively.

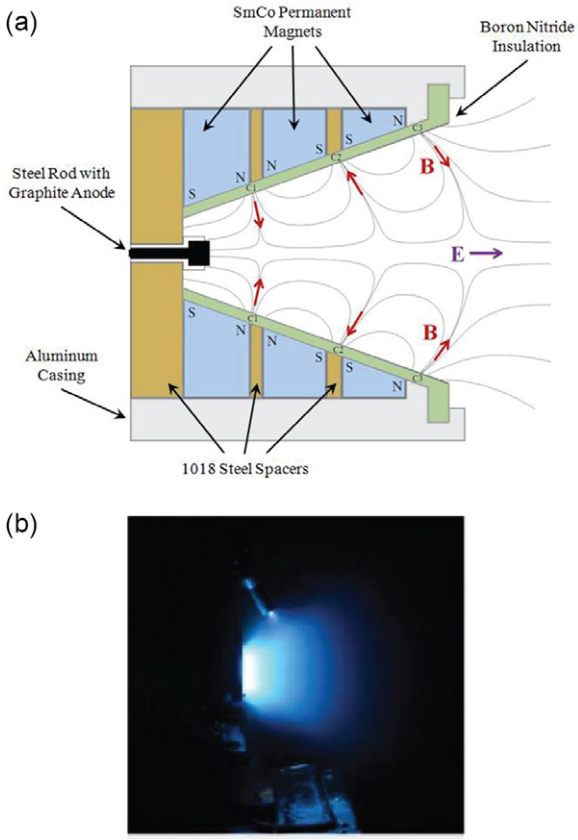

Figure 1. DCFT, developed by MIT. (*a*) Schematic of DCFT, (*b*) operation in high-current mode.

2. Experiment

2.1. Diverging cusped field thruster

Figure 1(*a*) provides a schematic of the DCFT. The acceleration channel in the DCFT has a diverging, cone shape that is lined with permanent samarium cobalt (SmCo) magnets of alternating polarity. These magnets create a cusped magnetic field profile that is largely in the axial direction, with radial components at the magnet interfaces. The magnetic field lines are assumed to form equipotential surfaces [4].

At the magnetic interfaces, the radially pointing magnetic field and axial electric field create a closed $\vec{E} \times \vec{B}$ electron drift, allowing for significant propellant ionization from electron bombardment. The closed electron drift also prevents electrons from directly reaching the anode, establishing a strong axial electric field that accelerates ions out of the thruster. In addition to these Hall thruster-like ionization and acceleration mechanisms, the cusped magnetic fields in these devices produce strong magnetic gradients that act on the charged particles within the thruster channel. These gradients result in a magnetic bottle effect for incoming electrons, trapping them between cusps where they mirror back and forth. Due to this

Table 1. DCFT operating condition during time-synchronized measurements.

Anode flow	830 μg s^{-1} Xe (8.5 sccm)
Cathode flow	150 μg s^{-1} Ar (4.75 sccm)
Anode potential	300 V
Anode current	0.49 A
Keeper current	0.50 A
Heater current	7.0 A

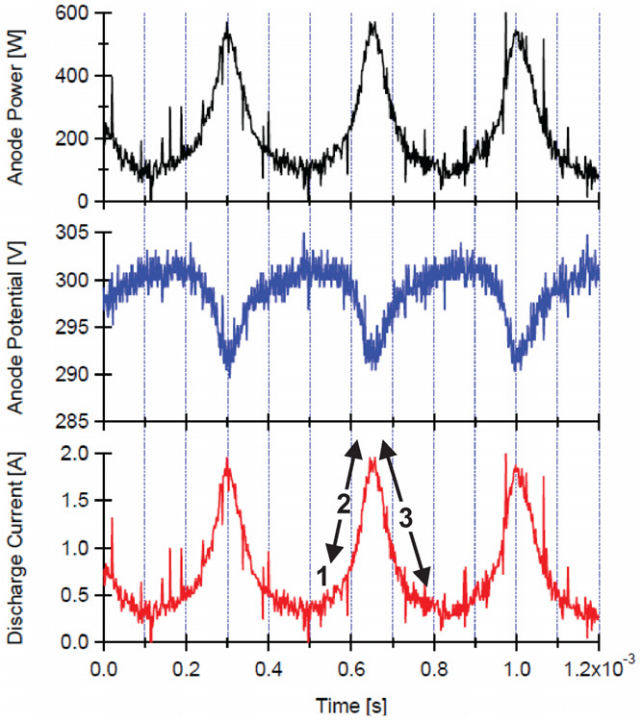

Figure 2. Anode current, voltage and power traces for the oscillatory operating mode of the DCFT. Numbers 1 to 3 in the lower trace describe the three phases within the current cycle.

magnetic mirror effect, the majority of charged particles (both ions and electrons) are prevented from reaching the thruster walls. This minimizes wall erosion, a limiting factor in thruster lifetime. The magnetic bottles also further mitigate electron mobility directly to the anode, and add to the propellant ionization efficiency from the electron $\vec{E} \times \vec{B}$ drift. Further details of the design, including the magnetic field topology, can be found elsewhere [17].

As described above, the DCFT tends to operate in either a high-current or low-current mode. The high-current mode is characterized by periodic oscillations in the discharge current, while the low-current mode is quiescent. This work focuses on the high-current mode, shown figure 1(*b*), with the operating condition described in table 1.

Based on the current trace in figure 2 and optical observations [8], the oscillatory nature of the high-current mode has been attributed to three distinguishable phases within each current cycle:

(1) Fast ionization of neutrals throughout the region accessible to the plasma.

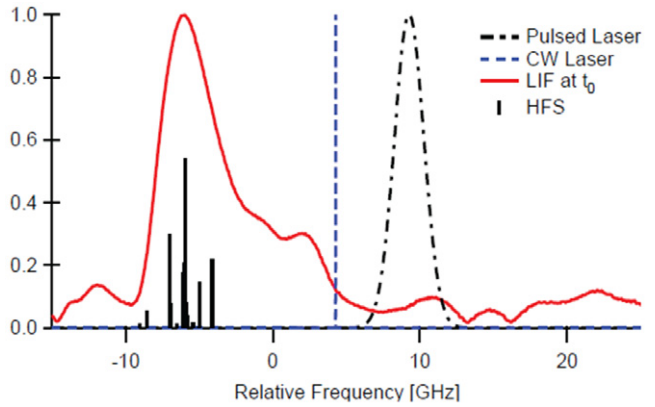

Figure 3. Fluorescence excitation lineshape at time t_0 at a position $X = -8$ mm, $Z = 0$ mm at the exit plane of the DCFT, as compared to the width of a typical CW laser and a pulsed dye laser. The hyperfine structure (HFS) of the transition is shown for reference.

(2) Evacuation of ions from the downstream end of the formed plasma, with simultaneous electron evacuation to the anode.
(3) Gradual refill of neutrals in the thruster channel.

As shown in figure 2, increases in discharge current are mirrored by slight decreases in anode potential, resulting in an anode power spikes that go as high as 570 W while the average power is 147 W.

While the DCFT discharge oscillations in some ways emulate the breathing mode of a Hall thruster [18, 19], the lower frequency (on the order of 3 kHz, compared to 15–20 kHz of a Hall thruster) and larger amplitude (greater magnitude than the steady-state current) of oscillations indicate that additional physics contributing to the ionization and acceleration processes in the DCFT are not yet fully understood. A time-resolved or time-synchronized CW-LIF method will help elucidate these mechanisms.

2.2. Experimental apparatus

Thruster LIF measurements are performed in the large vacuum chamber facility at the Stanford Plasma Physics Laboratory (SPPL). The base pressure in the chamber is 4×10^{-7} and 1×10^{-5} Torr with the DCFT running at nominal conditions (corrected for xenon).

Ion velocity measurements are accomplished by probing the $5d[4]_{7/2}$–$6p[3]_{5/2}$ electronic transition of Xe II at 834.72 nm. The lower state of this transition is metastable, while the upper state is shared by the $6s[2]_{3/2}$–$6p[3]_{5/2}$ transition at 541.92 nm [20], which is used in this study for non-resonant fluorescence collection. This transition has been used extensively throughout the electric propulsion community for time-averaged LIF velocimetry measurements [6, 21–23], including previous work on the DCFT [7]. Ion velocities are determined by measuring the Doppler shift of the absorbing ions [24].

Figure 3 provides a fluorescence excitation lineshape for time t_0 at a position of $X = -8$ mm, $Z = 0$ mm at the exit plane of the DCFT. Time t_0 refers to the point in the current cycle when the ac measurement of discharge current passes through

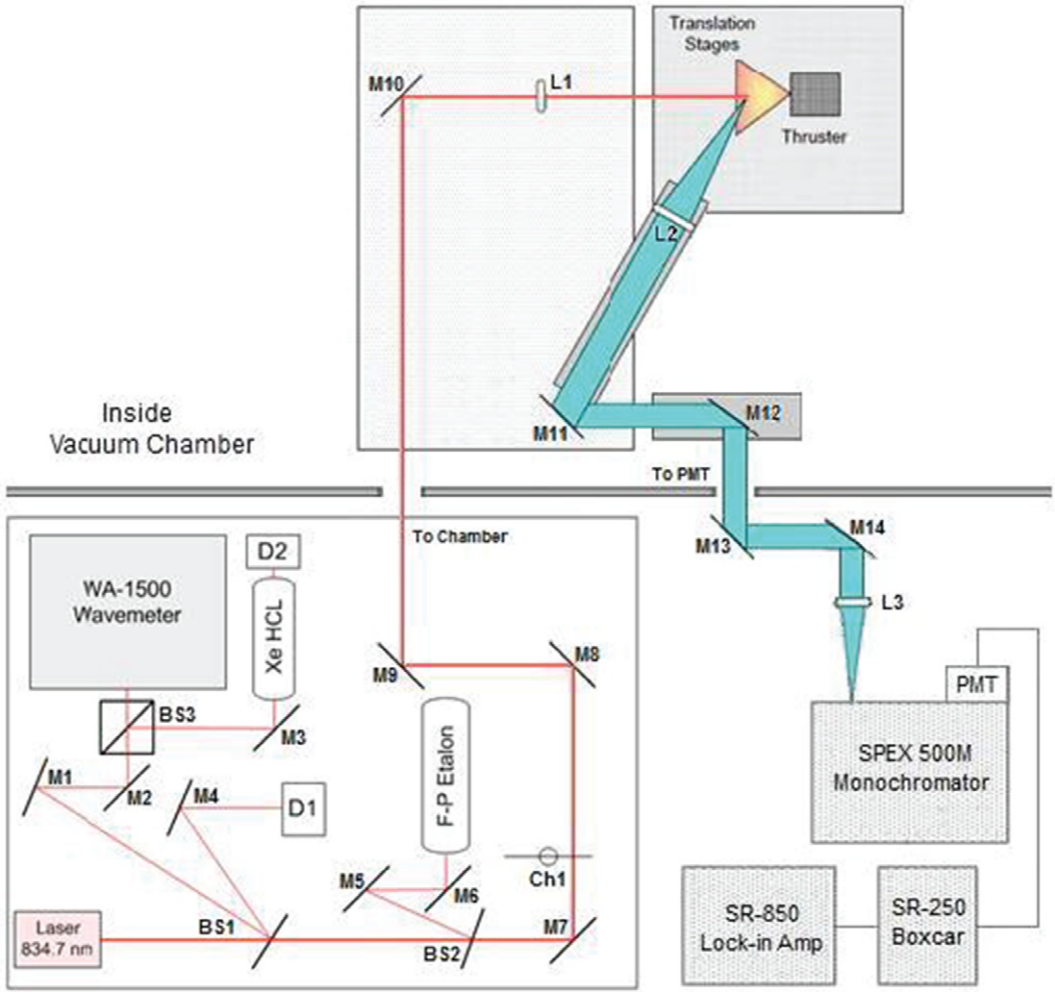

Figure 4. Top view diagram of the laser optical train and collection optics for time-synchronized thruster LIF measurements at SPPL; BS = beam Splitter; Ch = chopper; D = diode; L = lens; M = mirror.

zero with a positive slope. The linewidths for a CW and a pulsed dye laser, as well as the hyperfine structure (HFS) of the probed transition are also shown for reference. As mentioned previously, these line widths illustrate the need for a CW laser when resolving this spectral feature.

Figure 4 depicts the LIF optical system. The lower left-hand portion shows the probe optics before they enter the vacuum chamber. The laser is a New Focus Vortex TLB-6017 tunable CW diode laser, with a centre wavelength of 834.7 nm. The laser is typically scanned over an ∼40 GHz frequency range to encompass an entire spectral feature as well as a nearby reference line. The 10 mW beam is passed through several beam pick-offs for diagnostic purposes. The first beam pick-off directs a beam to a photodiode detector (D1) used to provide constant power feedback to the laser. The second beam is divided into two equal components by a 50–50 cube beam splitter. The first component is directed to a Burleigh WA-1500 wavelength meter used to monitor absolute wavelength. The second component is sent through a low-pressure xenon hollow cathode discharge lamp (HCL), that provides a wavelength reference through absorption of the neutral xenon $6s'[1/2]^0_1$–$6p'[3/2]_2$ transition at 834.68 nm [25, 26]. The second pick-off sends a beam to a Thorlabs SA200 Fabry–Perot etalon (F–P), with a 1.5 GHz free spectral range and finesse of 200. Combined with the absorption reference, the F–P etalon provides a high-resolution frequency measurement that gives a much more accurate measurement of wavelength than the wavemeter as the laser is swept during a scan.

The main portion of the beam is sent through a Stanford Research Systems SR540 mechanical chopper, rotating at 400 Hz for phase sensitive detection. Once inside the vacuum chamber, the beam is directed such that it probes axial ion velocities in the thruster. The fluorescence signal is collected by a 75 mm diameter plano-convex lens with a focal length of 250 mm. This lens is oriented 45° from the axial probe beam axis, a distance of 250 mm from the intersection with the probe beams, to minimize interactions with the plume (i.e. sputtering on the optics). The collected light is directed out of the vacuum chamber by a series of mirrors, and is then focused into a 750 mm focal length monochromator with a photomultiplier tube (PMT) by a second 75 mm diameter plano-convex lens with a focal length of 250 mm. The collection optics have a 1 : 1 magnification, which allows the spatial resolution of the measurements to be determined by the diameter of the probe beam (1 mm) and the image of the entrance slit (0.8 mm width

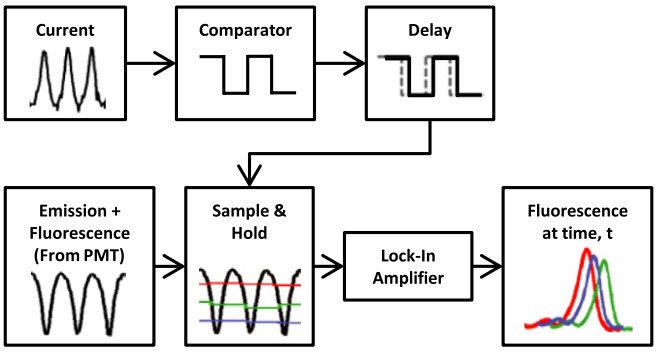

Figure 5. Block diagram of the sample-hold method of synchronizing the fluorescence trace to various times along a discharge current cycle.

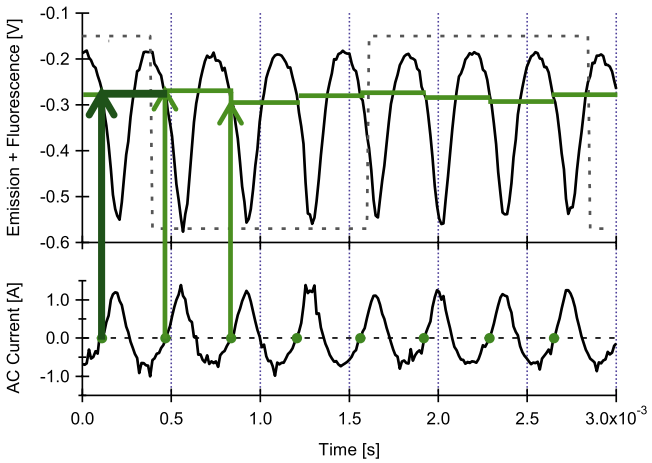

Figure 6. Raw PMT and ac current traces for the DCFT discharge. Arrows indicate the correlation between points in current cycle (bottom) and sample-held signal from the emission plus fluorescence trace (top) for time $= t_0$. Chopper frequency (- - - -) is shown for reference. Note: the emission plus fluorescence signal is negative due to the negatively applied bias on the PMT.

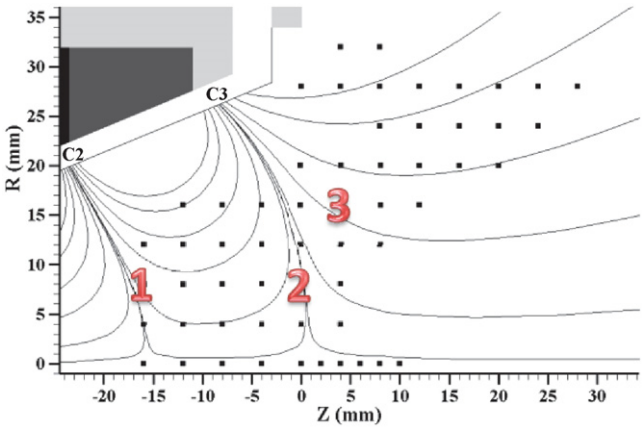

Figure 7. Positions of the three time-synchronized LIF measurements on the DCFT. Point 1 is located at $X = 8$ mm, $Z = -16$ mm; point 2 at $X = +8$ mm, $Z = 0$ mm; and point 3 at $X = +16$ mm, $Z = +4$ mm. Dots in figure represent time-averaged measurement locations from previous work.

by 0.2 mm height) that defines the collection optics solid angle. If sent directly into a lock-in amplifier, the resulting signal would be a conventional time-averaged measurement of the fluorescence excitation lineshape.

To synchronize the LIF signal in time to the discharge current, a sample-hold scheme is implemented between the PMT and the lock-in amplifier. The development and further details of this sample-hold scheme is described elsewhere [15]. Figure 5 provides a block diagram of the sample-hold method. Simultaneous measurements are made of the ac discharge current, absorption reference, etalon and emission plus fluorescence signal from the PMT, as the CW laser is scanned slowly in wavelength across the spectral feature. Due to the large background emission and associated noise, laser scans typically take on the order of 30 min to achieve adequate signal-to-noise for the fluorescence excitation lineshape.

The ac measurement of discharge current is fed into an LM339 comparator. Points where the current passes through zero with a positive slope trigger the comparator, resulting in a series of transistor–transistor logic (TTL) pulses with an approximately 50% duty cycle. The comparator signal and raw emission plus fluorescence signal from the PMT are then fed into an SRS SR-250 boxcar averager where the sample-hold function is performed.

For every positive slope in the comparator signal, the boxcar averager samples the PMT signal for a period of time defined by the gate width. The last sampled value of the PMT signal is held until the next comparator trigger, at which point the boxcar averager re-samples and holds the PMT signal. Figure 6 provides an example of how the zero point crossings of the ac discharge current (i.e. time $= t_0$) correlate to points in the sample-held emission plus fluorescence signal. This process is repeated throughout the length of the laser scan, resulting in the 'sample-held' signal.

The sample-held signal is then fed into an SRS SR-850 lock-in amplifier with the chopper reference frequency for phase sensitive detection, resulting in a fluorescence excitation lineshape synchronized to time t_0 in the current discharge cycle. To sample additional times along the current cycle, the built in time delay in the SR-250 is used to adjust the sample trigger before the laser scan is repeated.

3. Results and discussion

Figure 7 presents the three measurement locations used in this time-synchronized study of the DCFT. These points were chosen based on the time-averaged DCFT velocity measurements presented in previous work [7]. Note that these time-averaged measurements were taken at a different facility (the Air Force Research Laboratory at Edwards Air Force Base), with slightly different operating conditions. While these differences preclude us from making direct, quantitative comparisons to the time-synchronized velocity measurements, we believe that the operating conditions are sufficiently similar to reference time-averaged results when selecting time-synchronized measurement locations.

In the time-averaged measurements, the DCFT's high-current mode revealed axial acceleration beginning as deep as $Z = -12$ to -16 mm in the thruster channel (near the second cusp). This is in contrast to the quiescent, low-current

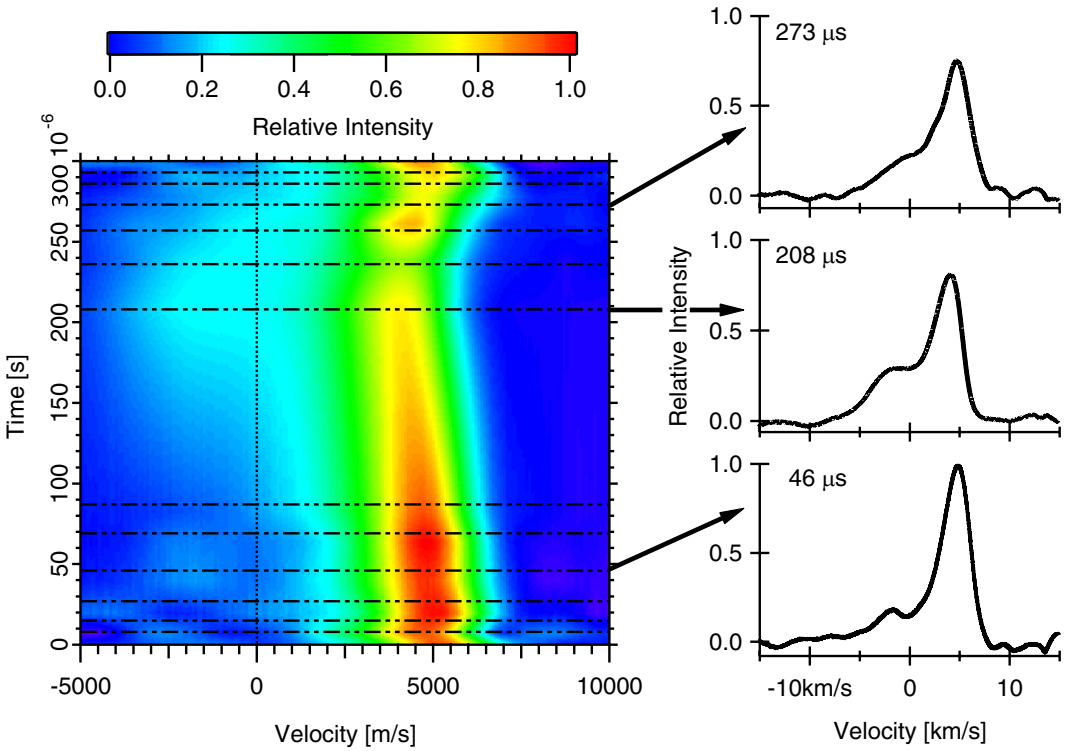

Figure 8. Variation of the ion velocity distributions for a single current cycle, measured at point 2, $X = -8$ mm, $Z = 0$ mm. Individual velocity distributions are shown for three phases of the current cycle (right), while the contour plot (left) shows the velocity distributions interpolated over the entire current cycle. Dashed lines (- - - -) represent measurement times.

mode of operation, in which the majority of the time-averaged ion acceleration was localized just inside the thruster exit plane (near the third cusp). From these observations, point 1 was chosen because it is in the brightest region of the plume, and is likely near a region of high ionization inside the thruster channel. This point is located at $X = +8$ mm, $Z = -16$ mm, inside the thruster channel near the separatrix defined by the second cusp, marked as C2. Point 2, at $X = +8$ mm, $Z = 0$ mm, is at the exit plane of the thruster near the outermost separatrix defined by the third cusp, C3. This point is near the region of highest measured potential drop, where the majority of ion acceleration begins. Point 3, at $X = +16$ mm, $Z = +4$ mm, is after the majority of the potential drop, where time-averaged measurements indicate that the ions continue ballistically outwards, perpendicular to the separatrix at cusp C3.

Figure 8 presents a contour plot of the time-synchronized ion velocity distributions at the exit plane of the thruster (point 2). This contour plot was achieved by interpolating lineshapes that were measured at 12 points in time along the current cycle. These points are shown as horizontal dashed lines across the figure. Note that measurements were not taken between 100–200 μs due to limitations in triggering the sample-hold circuit, and interpolated results between these times should therefore be interpreted with caution.

The three lineshapes on the right of figure 8 show ion velocity distributions that are typical of different phases along the current cycle at point 2. At the beginning of the current cycle, the lineshape is relatively narrow and the most probable (peak) velocities are on the order of 5 km s^{-1}. As the current reaches its maximum, a second peak forms in the velocity distribution, indicating the presence of near zero and negative velocity ions. As the current cycle progresses, this second peak diminishes until the distribution once again resembles that of the beginning of the current cycle.

Figures 9–11 summarize the most probable velocities and the full-widths at half-maximum (FWHMs) of the ion velocity distributions for the three measurement locations described in this work. At each of the measurement locations, the most probable velocities decline and reach their minimum as the discharge current is at its maximum. At point 1, in the ionization region, there appears to be no additional correlation between the FWHMs and the current cycle. At points 2 and 3, however, the widths of the velocity distributions increase with increasing discharge current. In the case of point 2, the increased width is due to the aforementioned second peak of lower velocity ions.

These correlation between velocity distributions and discharge current provide insight into the differing dynamics between the high current (oscillatory) and low current (quiescent) modes of the DCFT's operation. In time-averaged measurements [7], both the high- and low-current modes result in similar axial velocities along the contour of the ourtermost cusp (near the exit plane). However, in the low-current mode, the axial ion acceleration began between $Z = 0$ to 2 mm along the centreline, whereas the high-current mode had axial acceleration beginning deeper towards $Z = -5$ mm inside the thruster channel.

If we assume that ions are born at a fixed location near point 1, the wider distribution of the position of the high-current

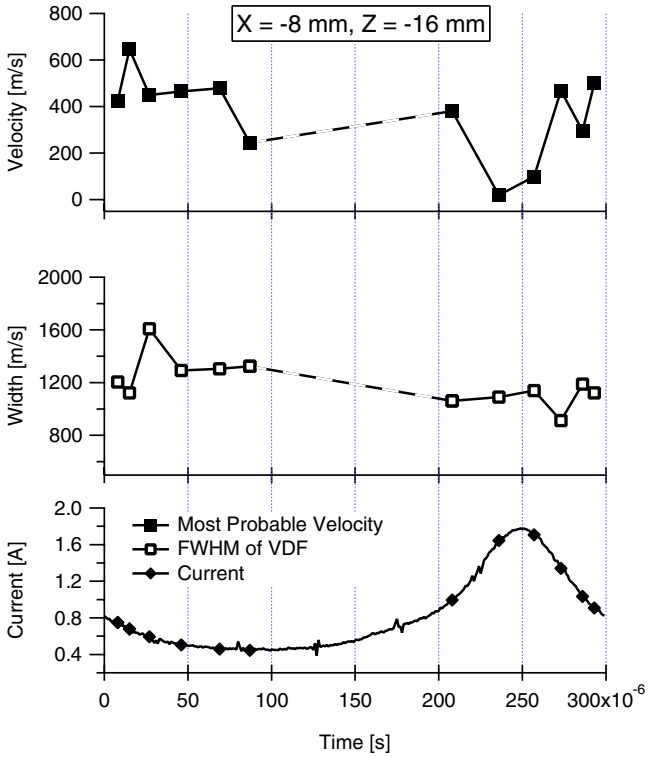

Figure 9. Measured most probable axial ion velocities and FWHMs of the measured velocity distributions as a function of the DCFT's discharge current at point 1 ($Z = -16$ mm, $X = -8$ mm).

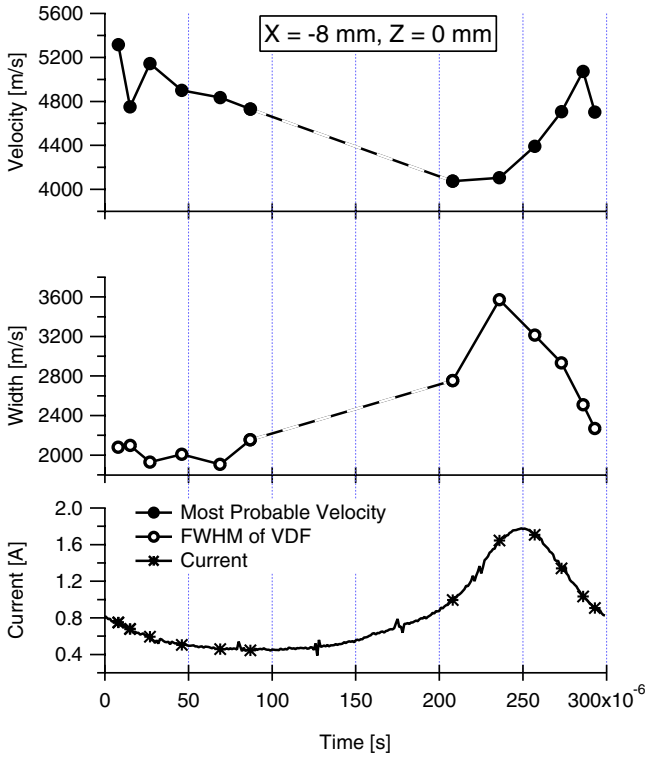

Figure 10. Measured most probable axial ion velocities and FWHMs of the measured velocity distributions as a function of the DCFT's discharge current at point 2 ($Z = 0$, $X = -8$ mm).

mode's initial acceleration may indicate a fluctuation of the position of the peak electric field. If the steepest potential drop (corresponding to the peak electric field) moves outwards in position as the discharge current reaches its peak, then subsequently recedes back towards $Z = -5$ mm as the current decreases, ions passing through each measurement location will experience varying degrees of acceleration depending on the phase within the current cycle. This hypothesis of a moving electric field can elucidate the aforementioned phenomena from figures 9–11.

As an example, the axial ion velocities at point 1 are somewhat higher earlier in the current cycle, corresponding to times when the wings of the electric field curve reach back to $Z = -16$ mm. If when the current increases, the peak electric field moves outwards, the ions measured remain near the thermal velocity at which they were born. Because the ion velocities are relatively low, the probed ions are likely to originate from virtually the same point (or a small subsection) of the ionization region. These ions would then experience the same acceleration, resulting in the FWHMs of the ion velocity distribution being relatively constant over the course of a current cycle.

At points 2 and 3, the probed ions have experienced successively larger portions of the acceleration due to the applied potential drop. Similar to point 1, when the potential drop is inside the thruster channel, ions at the measurement location have experienced a greater portion of their acceleration compared to when the potential drop moves outwards. At point 2, the resulting axial ion velocities reach their maximum of approximately 5 km s^{-1} and their minimum of 4.2 km s^{-1}. At point 3, the maximum most probable ion velocity reached is 11 km s^{-1}, and the minimum at this point is 8.9 km s^{-1}.

In contrast to point 1, the FWHMs of the velocity distributions at points 2 and 3 change substantially in phase with the changing discharge current. This implies that the ions are primarily created in the region near point 1 and subsequently travel to points 2 and 3 through a potential drop that varies with the gross discharge current. The variability of the FWHMs at points 2 and 3 may then be attributed to ions born at different times in the current cycle and then accelerated through a time varying potential drop.

In the case of point 2, the formation of secondary velocity peaks between 175–275 μs shown in figure 8 may reflect ion creation during a lull in the local electric field or even a reversal since the velocity of the second peak is negative. If it is indeed a potential reversal, a negative velocity of 2000 m s^{-1} only corresponds to a 3 eV ion energy, while the larger 5 km s^{-1} velocity of the primary peak represents 17 eV. The period of time during which the secondary velocity peaks form corresponds with the peak of the discharge current (occurring at approximately 250 μs) as shown in figure 10. The overall wider velocity distributions during this period may be indicative of a higher plasma density and plasma conductivity, which is consistent with increased discharge current.

Point 3 shows a similar pattern as point 2 (relative to point 1). However, only single velocity distribution peaks are evident, and they are wider than the primary peaks seen at the other two measurement locations. This is consistent with an overlap of the primary (high velocity) and secondary (near zero

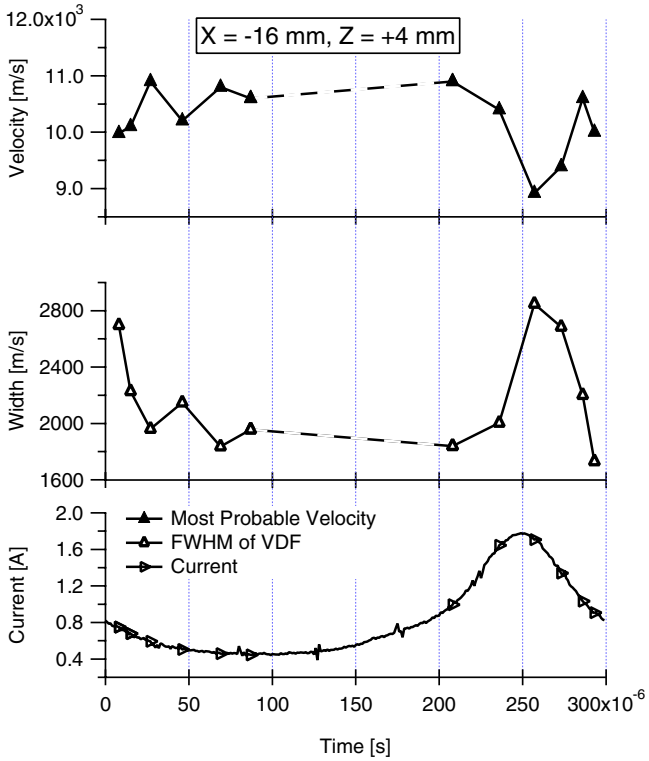

Figure 11. Measured most probable axial ion velocities and FWHMs of the measured velocity distributions as a function of the DCFT's discharge current at point 3 ($Z = +4$ mm, $X = -16$ mm).

velocity) distributions from point 2 due to the continued ion acceleration occurring between points 2 and 3. From figure 11 it is of note that although wider than the primary peaks of point 2, the overall FWHMs of the velocity distributions at point 3 are substantially less than that upstream at point 2 when the secondary, low-velocity peaks are present. This implies that ions at point 3 have experienced near the fullest spatial extent of the potential drop.

Overall, the results here strongly suggest that ions are formed in the region of point 1, are subsequently accelerated, and the characteristic distance over which the potential drop occurs between points 1 and 3 lengthens and shortens while the magnitude of the drop remains constant. This hypothesis is consistent with observations from time-averaged measurements as well as the temporally resolved data presented in this work; however, the sparse spatial extent of the data prevents conclusive determination of this hypothesis at this time.

4. Conclusions

This work presents a sample-hold with phase sensitive detection method of time-synchronized CW laser-induced fluorescence velocimetry. Time-synchronized axial ion velocity measurements are described for three points in the plume of the DCFT, operating in its oscillatory high-current mode. These measurements reveal that axial ion velocities in the DCFT are directly correlated to the phase of the discharge current oscillations, whereas the time-averaged velocity measurements are unable to resolve these dynamics.

At point 1 in the ionization region of the DCFT, the most probable axial ion velocity decreases as the discharge current peaks, and the widths of the velocity distributions remain relatively constant. At points 2 and 3 (at the exit plane and further into the plume), most probable axial ion velocities also show a decrease as the discharge current peaks. In these regions, there is also a correlation between the widths of the ion velocity distributions, which increase as the discharge current increases.

These time-synchronized velocity measurements support the hypothesis that the ion accelerating potential drop oscillates in position along the thruster axial direction. The data implies that the ionization region is relatively fixed point 1, with the subsequent potential drop extending towards point 3. We hypothesize that the position of the steepest potential drop oscillates in position due to changes in plasma density which in turn produce enhanced mobility, resulting in periods of high discharge current. Further spatial resolution of our time-synchronized measurements is necessary to derive changes in electric field. However, our hypothesis is consistent with the data presented here as well as previously reported time-averaged measurements.

These oscillations have similar characteristics to a Hall thruster breathing mode, which has been previously identified as an advancing and receding ionization front as neutrals are consumed. The differences in magnetic field configuration and oscillation frequency between the DCFT and traditional Hall thrusters, along with the limited spatial extent of the measurements presented here, warrant continued study in order to fully understand the discharge physics of these devices.

Acknowledgments

NM acknowledges the Science Mathematics and Research for Transformation (SMART) scholarship program for support of her research. Research at Stanford is funded through the Air Force Office of Scientific Research with Dr M Birkan as grant monitor.

References

[1] Khayms V and Martinez-Sanchez M 1996 Design of a miniaturized Hall thruster for microsatellites *Proc. 32nd AIAA/ASME/SAE/ASEE, Joint Propulsion Conf. and Exhibit (Lake Buena Vista, FL, 1–3 July 1996)* AIAA-96-3291

[2] Schmidt D P, Meezan N B, Hargus W A Jr and Cappelli M A 2000 *Plasma Sources Sci. Technol.* **9** 68

[3] Koch N, Harmann H P and Kornfeld G 2005 Development & test status of the THALES high efficiency multistage plasma (HEMP) thruster family *Proc. 29th Int. Electric Propulsion Conf. (Princeton, NJ, 31 October–4 November 2005)* IEPC-2005-297

[4] Raitses Y and Fisch N J 2001 *Phys. Plasmas* **8** 2579

[5] Courtney D G and Martinez-Sanchez M 2007 Diverging cusped-field Hall thruster (DCHT) *Proc. 30th Int. Electric Propulsion Conf. (Florence, Italy, 17–20 September 2007)* IEPC-2007-39

[6] MacDonald N A, Young C V, Cappelli M A and Hargus W A Jr 2012 *J. Appl. Phys.* **111** 093303

[7] MacDonald N A, Cappelli M A, Gildea S R, Martinez-Sanchez M and Hargus W A Jr 2011 *J. Phys. D: Appl. Phys.* **44** 295203

[8] Gildea S R, Matlock T S, Lozano P and Martinez-Sanchez M 2010 Low frequency oscillations in the diverging cusped-field thruster *Proc. 46th AIAA/ASME/SAE/ASEE Joint Propulsion Conf. & Exhibit (Nashville, TN, 25–28 July 2010)* AIAA-2010-7014
[9] Eckbreth A C 1996 *Laser Diagnostics for Combustion Temperature and Species* 2nd edn (London: Gordon and Breach)
[10] Newport Corporation Website, accessed 16 December 2011, www.newport.com
[11] Mazouffre S, Gawron D and Sadeghi N 2009 *Phys. Plasmas* **16** 043504
[12] Mazouffre S and Bourgeois G 2010 *Plasma Sources Sci. Technol.* **19** 065018
[13] Dannenmayer K, Kudrna P, Tichy M and Mazouffre S 2012 *Plasma Sources Sci. Technol.* **21** 055020
[14] MacDonald N A, Cappelli M A and Hargus W A Jr 2012 Development of a time synchronized CW-laser induced fluorescence measurement for quasi-periodic oscillatory plasma discharges *Bull. 65th Annual Gaseous Electronics Conf. (Austin, TX, 22–26 October 2012)* vol 57, No 8
[15] MacDonald N A, Cappelli M A and Hargus W A Jr 2012 *Rev. Sci. Instrum.* **83** 113506
[16] Pelissier B and Sadeghi N 1996 *Rev. Sci. Instrum.* **67** 3405
[17] Courtney D G, Lozano P and Martinez-Sanchez M 2008 Continued investigation of diverging cusped field thruster *Proc. 44th AIAA/ASME/SAE/ASEE Joint Propulsion Conf. & Exhibit (Hartford, CT, 21–23 July 2008)* AIAA 2008-4631
[18] Boeuf J P and Garrigues L 1998 *J. Appl. Phys.* **84** 3541
[19] Choueiri E Y 2001 *Phys. Plasmas* **8** 1411–26
[20] Hansen J E and Persson W 1987 *Phys. Scr.* **4** 602
[21] Manzella D H 1994 Stationary plasma thruster ion velocity distribution *Proc. 30th AIAA/ASME/SAE/ASEE Joint Propulsion Conf. & Exhibit (Indianapolis, IN, 27–29 June 1994)* AIAA-1994-3141
[22] Hargus W A Jr and Cappelli M A 2001 *Appl. Phys.* B **8** 961
[23] Mazouffre S, Gawron D, Kulaev V and Sadehgi N 2008 *IEEE Trans. Plasma Sci.* **36** 1967
[24] Demtroder W 1996 *Laser Spectroscopy: Basic Concepts and Instrumentation* (Berlin: Springer)
[25] Miller M H and Roig R A 1973 *Phys. Rev.* A **8** 480
[26] Moore C E 1958 *Atomic Energy Levels* vol II (Gaithersburg, MD: National Bureau of Standards)
[27] Barral S and Ahedo E 2009 *Phys. Rev.* E **79** 046401